

Investigation of Partial Discharge Characteristics in Mineral Oil Induced by Dibenzyl Disulfide

Amran Mohd Selva¹, Norhafiz Azis^{1*}, Muhammad Umair Tariq¹,
Mohd Zainal Abidin Ab Kadir¹, Jasronita Jasni¹ and Hidayat Zainuddin²

¹Advanced Lightning, Power and Energy Research Centre (ALPER), Universiti Putra Malaysia, 43400 UPM, Serdang, Selangor, Malaysia

²Faculty of Electrical Engineering, Universiti Teknikal Malaysia Melaka, Durian Tunggal 76100, Melaka, Malaysia

ABSTRACT

In this paper, an experimental study is carried out to investigate the partial discharge (PD) characteristic based on phase-resolved partial discharge (PRPD) and partial discharge inception voltage (PDIV) in mineral oil (MO) in the presence of dibenzyl disulfide (DBDS). MOs with different DBDS concentrations were aged at 150 °C for 5 days. Several parameters of the MO were measured, such as AC breakdown voltage, PDIV, apparent charge, average charge and PD repetition rate based on the needle-sphere, needle-plane and plane-plane electrode configurations. The AC breakdown voltage of aged MO displays a decrement pattern as the concentration of DBDS in the oil increases for all electrode configurations and gap distances. The average apparent charge of aged MO depicts an increment pattern in the presence of DBDS, whereas the PD repetition rate of aged MO displays variations of patterns for all electrode configurations. The PDIV of aged MOs shows an increment pattern at a 10 mm gap distance for all electrode configurations in the presence of DBDS. In contrast, the increment pattern of aged MOs is only observed for plane-plane electrode configuration at a 20 mm gap distance in the presence of DBDS. PDs occur predominantly

at negative peak half-wave between the 3rd to 4th quadrants and are undetectable at positive half-wave in base and aged MO for all electrode configurations.

ARTICLE INFO

Article history:

Received: 30 June 2024

Accepted: 24 December 2024

Published: 07 March 2025

DOI: <https://doi.org/10.47836/pjst.33.2.17>

E-mail addresses:

gs61085@student.upm.edu.my (Amran Mohd Selva)

norhafiz@upm.edu.my (Norhafiz Azis)

gs65418@student.upm.edu.my (Muhammad Umair Tariq)

mzk@upm.edu.my (Mohd Zainal Abidin Ab Kadir)

jas@upm.edu.my (Jasronita Jasni)

hidayat@utem.edu.my (Hidayat Zainuddin)

*Corresponding author

Keywords: Dibenzyl disulfide, partial discharge inception voltage, phased-resolved partial discharge

INTRODUCTION

The threat posed by the formation of corrosive sulphur on the transformer has

gained more attention over the past decades due to the increasing number of failures (Amaro, 2015; Cong et al., 2021; Khair et al., 2020; Vahidi & Tenbohlen, 2015). Generally, copper conductors can react with sulphur in mineral oil (MO) to form semi-conductive copper sulphide (Cu_2S) on the surface of the copper and insulating paper (eCIGRE, 2009; Yuan et al., 2022). Dibenzyl disulfide (DBDS) is an organic sulphur compound from the disulphide group commonly found in transformer's MO, which is considered a highly corrosive and a major cause of Cu_2S formation (Rehman et al., 2016). Cu_2S deposited on the winding can weaken the strength of the oil–paper insulation, and without mitigation, it can lead to failures (Hu et al., 2016; Yang et al., 2022). Sulphur compounds in the MO are usually present during the refining process of petroleum, which contains a high percentage of sulphur (Jadim et al., 2020; Rehman et al., 2016). The presence of Cu_2S and other corrosive by-products, i.e., copper oxide (Cu_2O), can accelerate the ageing process of oil-paper insulation (Cong et al., 2021). This phenomenon can lead to dielectric strength reduction, dielectric loss increment, and electrical discharge formation in oil-paper insulation due to the migration of Cu_2S (Liao et al., 2015; Yuan et al., 2022).

Dissolved gas analysis (DGA) is a common technique that can be used to analyse the issue related to corrosive sulphur in transformers (Amalanathan et al., 2023; Scatiggio et al., 2011). Other techniques that are used to evaluate the corrosive sulphur in transformer include gas chromatography electron capture detector, Fourier transform infrared spectroscopy, pyrolysis gas chromatography-mass spectrometry and covered conductor deposit (Jadim et al., 2020; Rehman et al., 2017). Fourier transform infrared spectroscopy can effectively detect the concentration of DBDS higher than 1.5% (Cong et al., 2018; Khan & Rajan, 2015). Gas chromatography-mass spectrometry is highly sensitive towards DBDS along with total and mercaptan sulphur. The combination of these techniques with DGA can be useful to understand the migration of DBDS (Toyama et al., 2009). Presently, relevant international test standards can be used to detect the corrosivity in oil, including DIN 51353, ISO 5662, ASTM D1275A, ASTM D1275B and IEC 62535-2008 standards. The corrosiveness of MO can be evaluated based on ASTM D 130/TP 154 standard. However, different standards may lead to different interpretations of the condition of MO (Khair et al., 2019; Gao et al., 2019). Partial discharge (PD), frequency domain spectroscopy, frequency response analysis, polarisation depolarisation current, and recovery voltage are among alternative methods that can be used to evaluate the corrosive sulphur issue in oil-paper insulation (Bramantyo et al., 2014; Cong et al., 2024; Flora & Rajan, 2016).

The phenomenon of PD in dielectric insulating fluid is inherently random and involves complex interactions with electrical, mechanical and thermal factors (Dixit & Samarasinghe, 2019; Jin et al., 2015). PD events can arise from localised electric field intensification due to the amplitude and waveform of the applied voltage, the distance between electrodes, the configuration of the electrodes, conductor defects, floating particles, bubbles and contaminants in dielectric insulating fluid (Sima et al., 2013). In dielectric

insulating fluid, the PD occurrence is more complex as electrons are unstable, forming and collapsing unpredictably under the influence of the electric field. Consequently, rapid bursts of PD pulses in dielectric insulating fluids can occur with increasing magnitude, which can be challenging to detect. The initiation of discharges in a low-density region of dielectric insulating fluids depends on the availability of electrons. The electrons can trigger an avalanche effect and subsequently streamer occurrence.

Several studies have previously been carried out to examine the impact of moisture and contaminants on the PD properties of MO. These contaminants can exist as either floating conductive or non-conductive particles. Other works also examine the PD due to ageing and oxidation by-products of oil-paper insulation. It is found that these contaminants can affect the PD properties of the MO, although the extent of its impact can vary depending on the voltage level and chemical composition. Previous studies demonstrate that moisture can reduce the PD magnitude at low voltage, which leads to a high partial discharge inception voltage (PDIV) (Liu et al., 2014; Pattanadech & Muhr, 2016). Conversely, at high voltage, the PD magnitude increases with the increment of the moisture. The presence of moisture can significantly affect the PD repetition rate. The PD pattern also shows apparent changes due to the increment of moisture. Another study shows that the PD induced by the bubbles in MO is predominantly concentrated at the negative half-wave (Tang et al., 2018). Additionally, negative PD generally exhibits a higher apparent charge than positive PD, regardless of whether the MO is flowing or stationary.

Generally, depending on their size and concentration, metallic particles can reduce the PDIV. It can also act as an initiation point for discharges and reduce AC breakdown voltage in the MO (Ma et al., 2019). Furthermore, the metallic particle can change PD characteristics and magnitude. Large particles can increase PD magnitude by offering more sites for discharges to initiate, while small particles may have less effect depending on their dispersion and interaction with the electric field. Research has shown that metallic particles can cause different PD patterns and discharge phenomena, impacting the oil-paper insulation's overall condition (Tang et al., 2018).

The main motivation of this study is to investigate the impact of DBDS on the dielectric strength and PD characteristics of MO. The aim of the research is to examine the feasibility of PD as an alternative technique to detect DBDS-induced corrosion in MO. First, the AC breakdown of base and aged MOs at different DBDS concentrations for needle-sphere, needle-plane and plane-plane electrode configurations at 10 mm and 20 mm gap distances are recorded and analysed. Next, the PD magnitude in terms of apparent charge (Q_{IEC}), average charge (Q_{AVG}), PD repetition rate and PDIV in MOs at various DBDS concentrations are compared with the base oil. PRPD of MOs at various DBDS concentrations is acquired for different electrode configurations and gap distances to investigate the shape and PD intensity, $H_n(\varphi)$.

METHODOLOGY

Material Preparation for Thermal Ageing

The overall framework of this experimental study can be seen in Figure 1. A test cell made of perspex with a height, width and depth of 2,200 mm × 100 mm × 100 mm and a volume capacity of 2,200 ml was used to investigate the PD characteristics in MO in the presence of DBDS. For needle-sphere electrode configuration, a needle with a tip radius of 200 μm was used as the high potential electrode, whereas a sphere with a diameter of 12.7 mm was set as the ground electrode. For needle-plane electrode configuration, a needle with a tip radius of 200 μm was used as the high potential electrode, whereas a plane with a diameter of 50 mm was set as the ground electrode. A plane with a 50 mm diameter was used as the high potential and ground electrodes for plane-plane electrode configuration. These configurations are designed to study PD characteristics. The needle-sphere and needle-plane configurations create a concentrated electric field at the needle's tip, intensifying electric field stress and simulating conditions for PD initiation. On the other hand, the plane-plane configuration offers a more uniform electric field, typically used to examine discharge activities under evenly distributed field conditions. The specifications of MO, Kraft paper, and copper conductor used in this experiment can be obtained from Selva et al. (2024). DBDS with 246.39 g/mol was used in this study to induce corrosivity in oil.

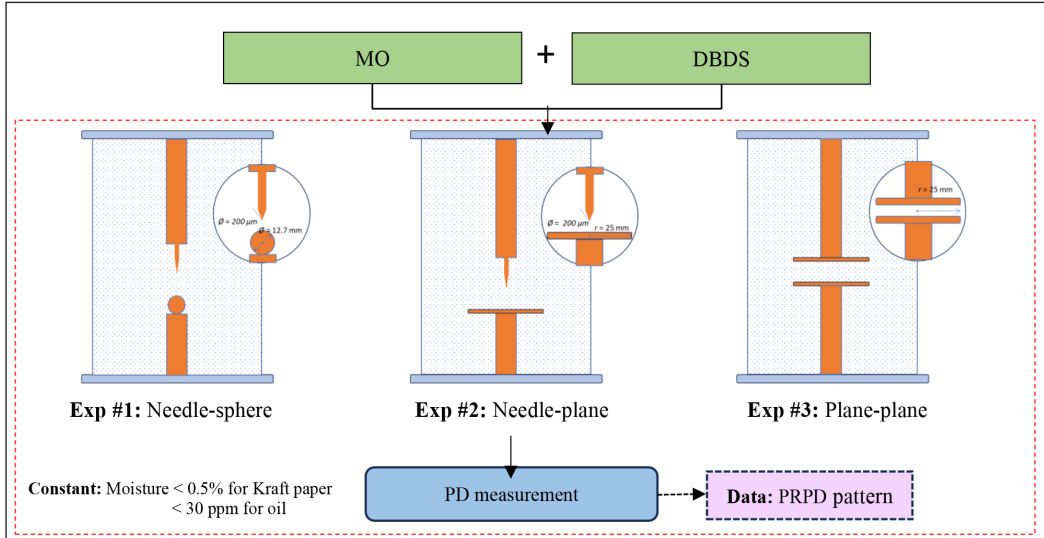


Figure 1. Overall framework of the study

In total, 4 samples were prepared for this experiment to investigate the scenarios described in Table 1. First, the MO was filtered based on a membrane filter with a pore size of 0.25 μm. Next, MO was dried in an air-circulating oven for 96 h at 85°C. Similarly, the

Kraft paper was dried for 48 hours at 105°C. The MO was subjected to nitrogen purging for 20 minutes to further reduce the moisture content. The moisture content of the Kraft paper and MO were determined based on the IEC 60814 standard, whereby the values were 0.1287% and 17 ppm. The copper conductor with height, width and depth of 100 mm × 15 mm × 3 mm was wound with dried Kraft paper with a width of 25 mm width for 10 layers in a half-lap configuration similar to the arrangement in the transformer, where half of the paper was overlapped with the next turn and in direct contact with the copper conductor as shown on Figure 2. DBDS was added to the 1,000 ml of MO at different weights of 1 g, 5 g and 10 g and mixed using a magnetic stirrer to create concentrations of 1,000, 5,000 and 10,000 ppm, respectively, as shown in Table 1. The wrapped copper conductor was then added to the oil with DBDS at room temperature for 12 hours. The samples were then thermally aged under sealed conditions for 5 days at 150°C in an oven with a closed cap to reduce contact with oxygen from the atmosphere.

Table 1
Experimental condition of the study

Experiment	Description	DBDS Weight (g)	DBDS concentration (PPM)	Experimental condition
1	Base MO	0	0	150°C, 5 days
2	Aged MO-DBDS#1	1	1,000	
3	Aged MO-DBDS#2	5	5,000	
4	Aged MO-DBDS#3	10	10,000	

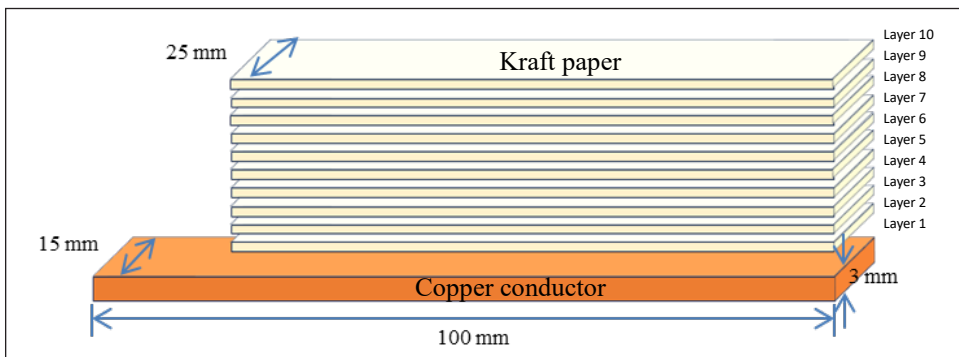


Figure 2. The cross-sectional area of paper-wrapped copper

Experimental Procedure

The test setup for AC breakdown voltage is shown in Figure 3. A PD-free transformer provided AC voltages up to 100 kV at 50 Hz. A protective resistor of 2 kΩ was placed to limit the breakdown current. The gap distances between the electrodes were set at 10 mm

and 20 mm. A small gap results in strong electric fields, which increases the likelihood of PDs, especially around sharp points in needle electrode configuration. This also reduces the voltage required to initiate PDs due to higher field stress. In contrast, a large gap reduces the field intensity and raises the inception voltage (Wang, 2011). These variations help in comparing how concentrated fields in needle-plane and needle-sphere electrode configurations differ from uniform fields in plane-plane electrode configuration, revealing valuable insights into insulation design and discharge characteristics under different conditions. The MO was poured carefully into the test cell and allowed to stand for at least 15 minutes before the voltage was applied. The voltage automatically increased by 1 kV per step until it broke down. The AC breakdown for each type of MO was recorded as a reference for the threshold voltage of PD measurement.

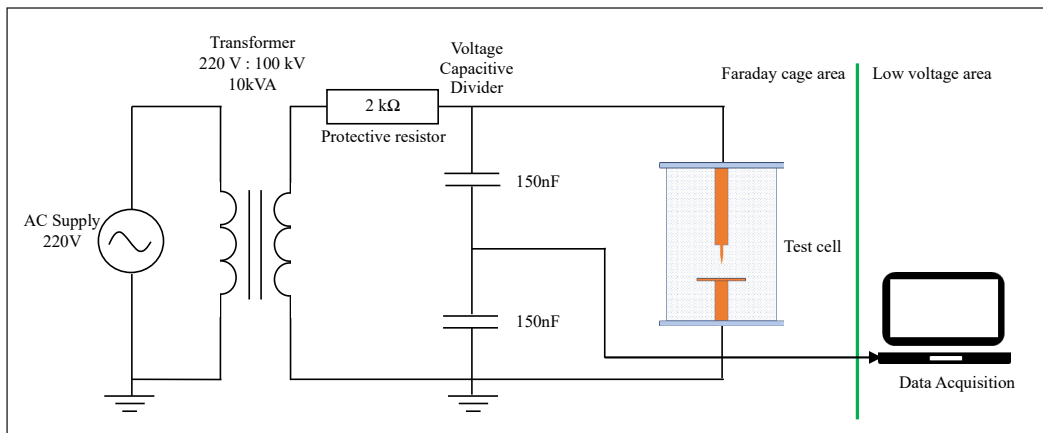


Figure 3. Schematic diagram of AC breakdown measurement

The PD characteristics were acquired through a conventional PD coupling circuit in accordance with IEC 61294 and IEC 60270 standards. The schematic diagram of PD measurement can be seen in Figure 4. A coupling capacitor of 1 nF was used to provide a displacement current. The setup can provide additional information about the test voltage needed for the PRPD analysis. The maximum apparent charge of the background noise was registered at less than 600 fC. The PD detection system was calibrated based on the IEC 60270 standard, where an external charge of 20 pC value was injected into the system, which simulated a PD event, and its amplitude was used as a reference scale. The 70% and 90% AC breakdown voltage for each of the MO samples was used as a reference for the threshold voltage for PD measurement. The step voltage of 1 kV was applied automatically via an AC high voltage controller until it reached the peak voltage, whereby the time interval between each of the voltages was set to 30 s. A wide bandwidth PD detector recorded the PD signals continuously for 1 min once it reached the required voltage. In this study, the

lowest voltage at which the maximum amplitude of PD signals reached 10 pC was defined as the PDIV. The PD charge (q) was determined through the integration of the PD current ($i(t)$) over the PD time interval, as shown in Equation 1.

$$q = \int_{t_1}^{t_2} i(t) dt \quad [1]$$

Here, q represents the charge, $i(t)$ denotes the current, and t_1 and t_2 indicate the start and end times of the discharge pulse, respectively.

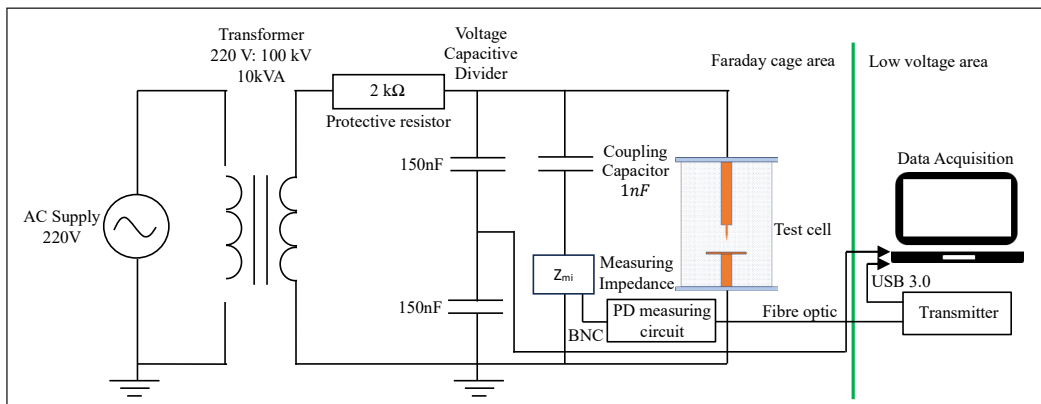


Figure 4. Schematic diagram of partial discharge measurement

RESULTS AND DISCUSSION

Effect of DBDS on AC Breakdown Voltage

The reductions of AC breakdown voltages for aged MO in the presence of DBDS are quite apparent for needle-sphere and needle-plane electrode configurations compared to plane-plane electrode configuration for a 10 mm gap distance, as shown in Figure 5. For all electrode configurations, the highest reduction of AC breakdown voltage is found for aged MO in the presence of a DBDS concentration of 5,000 ppm. The highest percentages of AC breakdown voltage reductions for aged oils under needle-sphere, needle-plane and plane-plane electrode configurations are 42.0%, 33.3% and 8.1%.

The AC breakdown voltage reduction patterns for aged MO at a 20 mm gap distance are quite similar for all electrode configurations in the presence of DBDS, as shown in Figure 6. Similar to the 10 mm gap distance, the AC breakdown voltage reduction of aged MO is the highest at a DBDS concentration of 5,000 ppm. The aged MO in the presence of DBDS experiences the highest percentages of AC breakdown voltage reductions of 21.9%, 17.1% and 18.3% under needle-sphere, needle-plane and plane-plane electrode

configurations. Based on the previous finding by Cong et al. (2018), the addition of DBDS can increase the moisture content in aged MO, which results in the reduction of the AC breakdown voltage and increment of the dielectric loss.

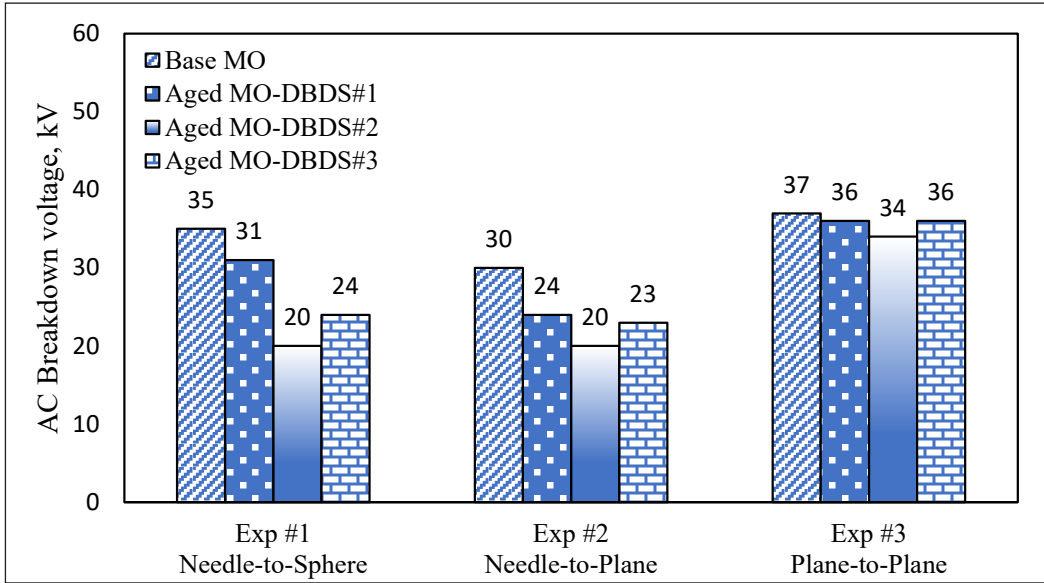


Figure 5. The AC breakdown voltage of MO in the presence of DBDS at a 10 mm gap distance

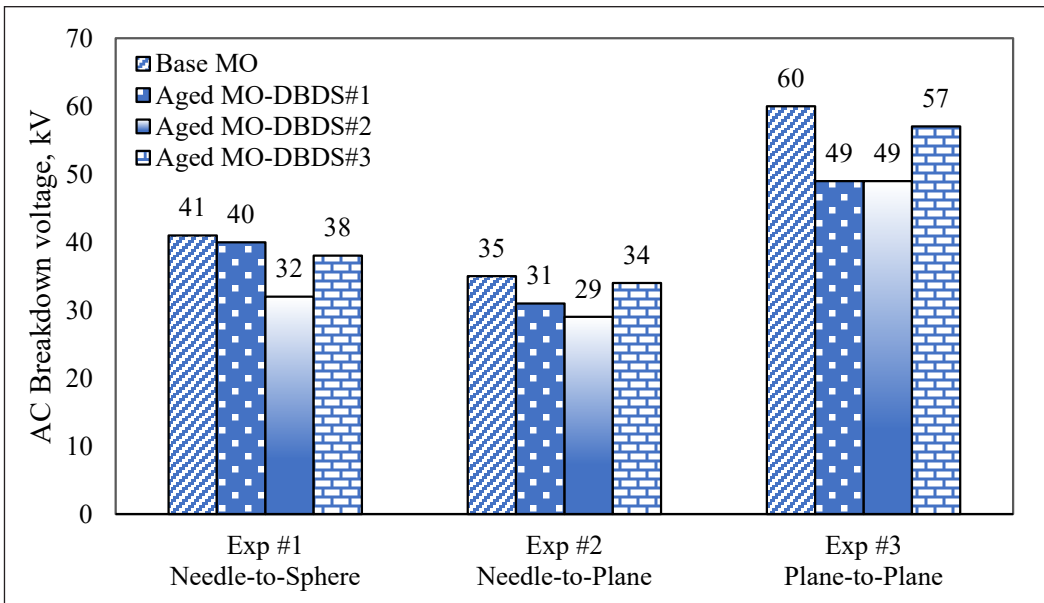


Figure 6. The AC breakdown voltage of MO in the presence of DBDS at a 20 mm gap distance

Effect of DBDS on Partial Discharge Characteristics

The PD apparent charge, average charge and PD repetition rate that are recorded from 70% to 80% of peak voltage for 1-minute intervals are obtained based on the mean of the datasets for base and aged MOs in the presence of DBDS. There is a clear reduction pattern for an apparent charge of aged MO with the increment of DBDS concentration at a 10 mm gap distance for needle-sphere electrode configuration, as shown in Figure 7. The highest reduction percentage for an apparent charge of aged MO is found at a DBDS concentration of 1,000 ppm with 83.5%. The average charge of aged MO shows a slight increment pattern as the DBDS concentration increases. The average charge of aged MO experiences the highest percentage of increment up to 50.2% at DBDS concentrations of 5,000 ppm and 10,000 ppm. The PD repetition rate of aged MO initially decreases to 50.0% as the DBDS concentration increases to 5,000 ppm. As the DBDS concentration increases to 10,000 ppm, the PD repetition rate of aged MO slightly increases.

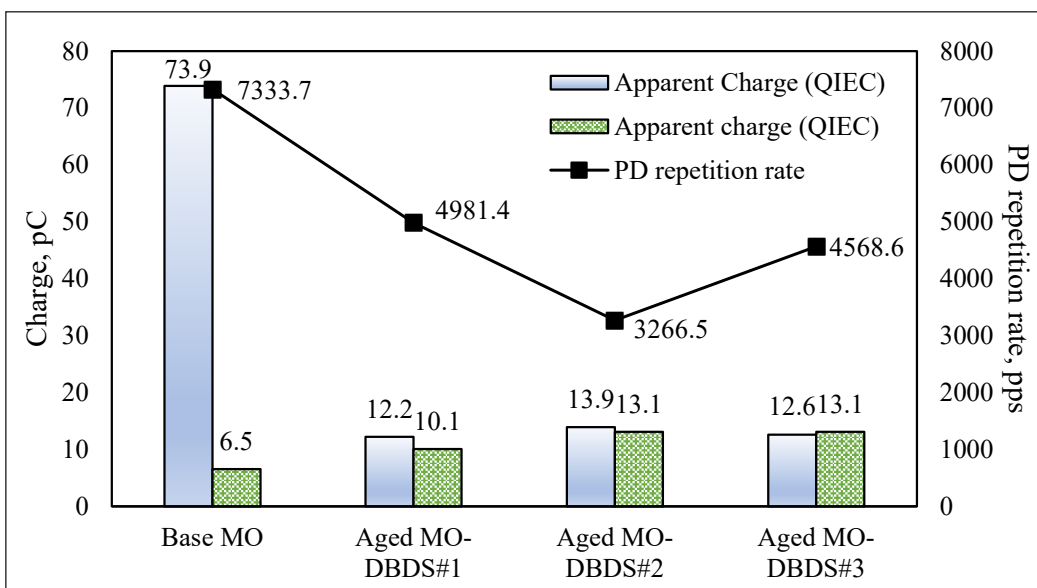


Figure 7. Comparison of the partial discharge characteristics for the base and aged MOs in the presence of DBDS based on needle-sphere electrode configuration at a 10 mm gap distance

At a 20 mm gap distance, the apparent charge of aged MO shows a slight increment pattern as the DBDS concentration increases for needle-sphere electrode configuration, as shown in Figure 8. The highest increment percentage for an apparent charge of aged MO is 53.5% at a DBDS concentration of 10,000 ppm. Similarly, the average charge of aged MO shows a slight increment pattern whereby the highest increment percentage occurs at a DBDS concentration of 10,000 ppm with 61%. The PD repetition rate of aged MO increases steadily with the increment of DBDS concentration, whereby the highest percentage of increment can be up to 40.4% at DBDS concentration of 10,000 ppm.

The skewness and kurtosis were calculated based on Janani et al. (2020). Table 2 shows the skewness and kurtosis of PD apparent charge, average charge, and PD repetition rate for needle-sphere electrode configuration. At a 10 mm gap, the skewness of apparent charge for all MO samples stays low, which indicates consistent symmetry, while kurtosis increases, especially for aged MOs, in the presence of DBDS, which suggests more discharge activity. The average charge shifts from negative to positive skewness as DBDS is introduced, which indicates a change in data symmetry, and the kurtosis slightly peaks for aged MO at a DBDS concentration of 10,000 ppm. The PD repetition rate skewed slightly for aged MOs in the presence of DBDS, with some left-skewed data, and kurtosis increases for aged MOs at DBDS concentrations of 5,000 and 10,000 ppm, respectively, which indicates more irregular distributions.

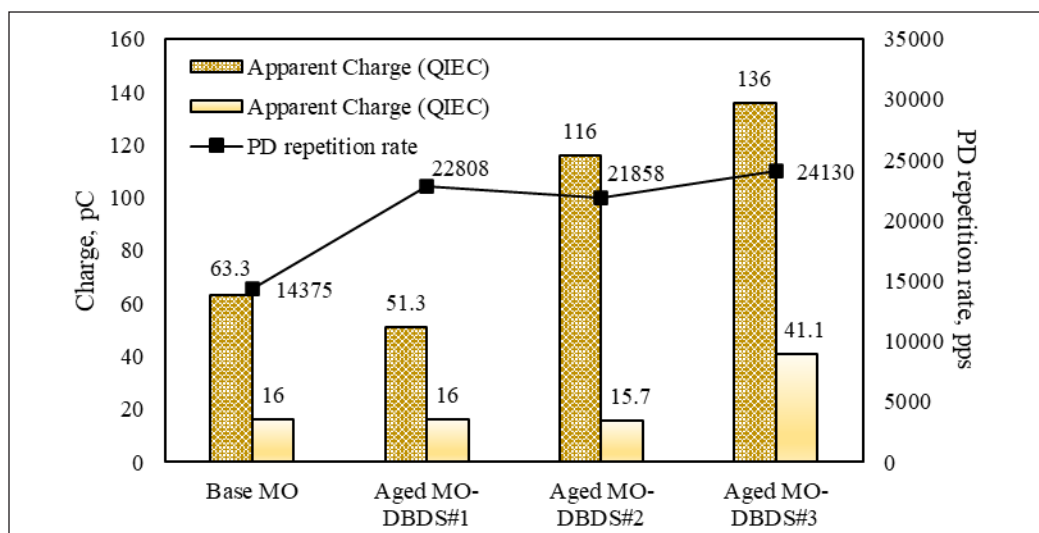


Figure 8. Comparison of the partial discharge characteristics for the base and aged MOs in the presence of DBDS based on needle-sphere electrode configuration at 20 mm gap distance

At a 20 mm gap, the skewness of apparent charge for all MO samples remains low and stable, which indicates minimal effect of the DBDS, while kurtosis peaks for aged MO at DBDS concentration of 1,000 ppm, which suggests more extreme values as compared to other MO samples with high DBDS concentrations. The average charge skewness shifts from left-skewed in base MO to more negative for aged MOs in the presence of DBDS, which shows an increment of the asymmetry, while the kurtosis peaks for aged MO at DBDS concentration of 5,000 ppm, which indicates a concentrated distribution. The PD repetition rate skewness of all MO samples maintained low with minor left-skew, and the kurtosis is high for base MO and peaks for aged MO at a DBDS concentration of 10,000 ppm, which indicates concentrated distributions for both MO samples.

Table 2
Skewness and kurtosis analyses for apparent charge, average charge and partial discharge repetition rate under needle-sphere electrode configuration

Parameter	Apparent charge			Average Charge			PD repetition rate					
	Base MO	Aged MO-DBDS#1	Aged MO-DBDS#2	Base MO	Aged MO-DBDS#1	Aged MO-DBDS#2	Base MO	Aged MO-DBDS#1	Aged MO-DBDS#2	Aged MO-DBDS#3		
Skewness - 10 mm	1.9	1.1	-4.3	5.4	-1.4	-0.3	1.3	2.3	-0.1	0.6	-3.7	-2.7
Kurtosis - 10 mm	6.4	-0.3	18.4	29.7	0.7	-0.9	0.4	4.3	-0.3	-0.6	17.8	13.4
Skewness - 20 mm	6.8	12.7	3.5	1.3	-1.5	-0.2	-2.3	-1.8	-3.5	-0.8	-1.0	-4.6
Kurtosis - 20 mm	55.0	172.5	11.0	2.4	0.8	-0.3	5.1	1.9	14.0	2.9	6.1	26.8

At a 10 mm gap distance, the increment pattern for an apparent charge of aged MO is not apparent as the DBDS concentration increases for needle-plane electrode configuration, as shown in Figure 9. The highest percentage of increment for an apparent charge of aged MO is 7.9% at DBDS concentrations of 5,000 and 10,000 ppm. The average charge of aged MO shows a fluctuation pattern whereby the percentage of differences with base MO varies between 1.9% and 61% as the DBDS concentration increases to 10,000 ppm. The PD repetition rate of aged MO initially decreases as the DBDS concentration increases to 5,000 ppm. It increases to 58.7% as the DBDS concentration increases to 10,000 ppm.

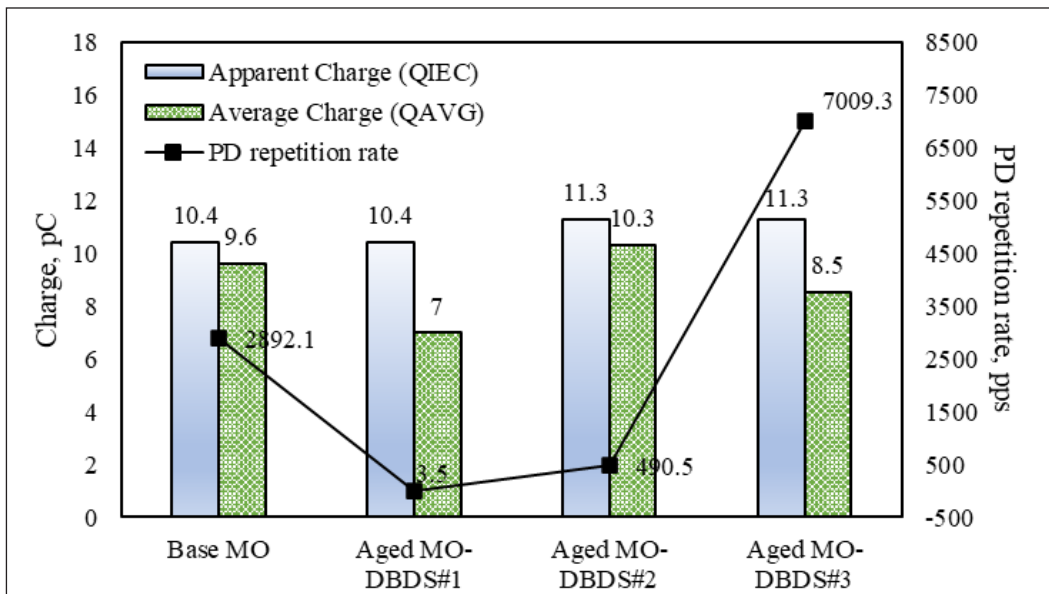


Figure 9. Comparison of the partial discharge characteristics for the base and aged MOs in the presence of DBDS based on needle-plane electrode configuration at a 10 mm gap distance

There is no clear pattern for an apparent charge of aged MO as the DBDS concentration increases at a 20 mm gap distance for needle-plane electrode configuration, as shown in Figure 10. The apparent charge of aged MO maintains close to 12 pC as the DBDS concentration increases by 10,000 ppm. A similar pattern is found for the average charge of aged MO, whereby it slightly increases as the DBDS concentration increases to 1,000 ppm. It decreases to 9.8% as the DBDS concentration increases to 10,000 ppm. There is a clear reduction pattern for the PD repetition rate of aged MO as the DBDS concentration increases at a 10 mm gap distance for needle-sphere electrode configuration. The highest percentage of reduction for PD repetition rate of aged MO is found at DBDS concentration of 1,000 ppm with 84.5%.

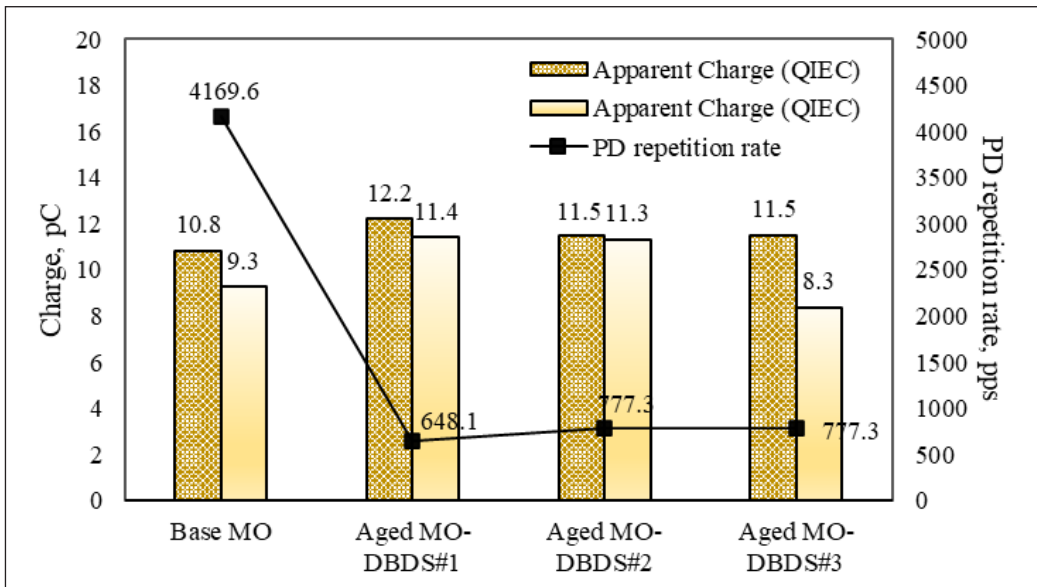


Figure 10. Comparison of the partial discharge characteristics for the base and aged MOs in the presence of DBDS based on needle-plane electrode configuration at 20 mm gap distance

Table 3 shows the skewness and kurtosis of apparent charge, average charge, and PD repetition rate for needle-plane electrode configuration. At a 10 mm gap, the skewness of apparent charges for all MO samples remains low and stable, which indicates consistent symmetry. The kurtosis of MO decreases, indicating a transition from extreme to uniform distributions as the DBDS concentration increases. The skewness of the average charge for all MO samples stays consistent, with base MO slightly left-skewed, while the kurtosis of aged MO decreases as the DBDS concentration increases, which suggests a shift from a peak to a flat distribution. The PD repetition rate skewness for all MO samples remains stable and slightly left-skewed, while the kurtosis for aged MO decreases in a similar pattern as the apparent charge.

At a 20 mm gap, the skewness of apparent charges for all MO samples stays low and consistent, while the kurtosis of aged MO decreases as the DBDS concentration increases to 10,000 ppm, which suggests a more uniform distribution as compared to base MO. The average charge skewness shifted from left-skewed for base MO to right-skewed as the DBDS concentration increased for aged MO, with the kurtosis showing initial peaks and eventually remaining flat as the DBDS concentration increased, which indicates uniform distribution. The PD repetition rate skewness for all MO samples stayed mostly negative, which indicates a right-skewed tendency, with high kurtosis in base MO and aged MO at a DBDS concentration of 5,000 ppm, which suggests extreme data.

Table 3
Skewness and kurtosis analyses for apparent charge, average charge and partial discharge repetition rate under needle-plane electrode configuration

Parameter	Apparent charge			Average Charge			PD repetition rate					
	Base MO	Aged MO- DBDS#1	Aged MO- DBDS#2	Base MO	Aged MO- DBDS#1	Aged MO- DBDS#2	Base MO	Aged MO- DBDS#1	Aged MO- DBDS#2	Aged MO- DBDS#3		
Skewness - 10 mm	16.5	6.5	9.6	5.0	-3.7	1.2	-1.3	1.9	-5.7	7.0	-5.2	-4.0
Kurtosis - 10 mm	279.9	43.1	96.1	24.3	13.8	-0.1	0.0	2.1	50.4	48.3	35.9	19.4
Skewness - 20 mm	9.9	6.8	4.8	0.9	-1.8	-1.2	1.4	0.7	-4.4	0.3	-3.1	-2.6
Kurtosis - 20 mm	98.0	45.4	26.9	2.4	1.8	0.2	1.1	-0.9	23.1	-0.6	23.5	10.1

At a 10 mm gap distance, there is no clear pattern for an apparent charge of aged MO as the DBDS concentration increases for plane-plane electrode configuration, as shown in Figure 11. The apparent charge of aged MO fluctuates between 6.1% and 11.5% compared to base MO once the DBDS increases to 10,000 ppm. There is a slight increment pattern for the average charge of aged MO, whereby the highest percentage of increment is 34.7% at a DBDS concentration of 10,000 ppm. The PD repetition rate of aged MO initially decreases to 77.2% as the DBDS concentration increases to 5,000 ppm. It slightly increases as the DBDS concentration increases to 10,000 ppm.

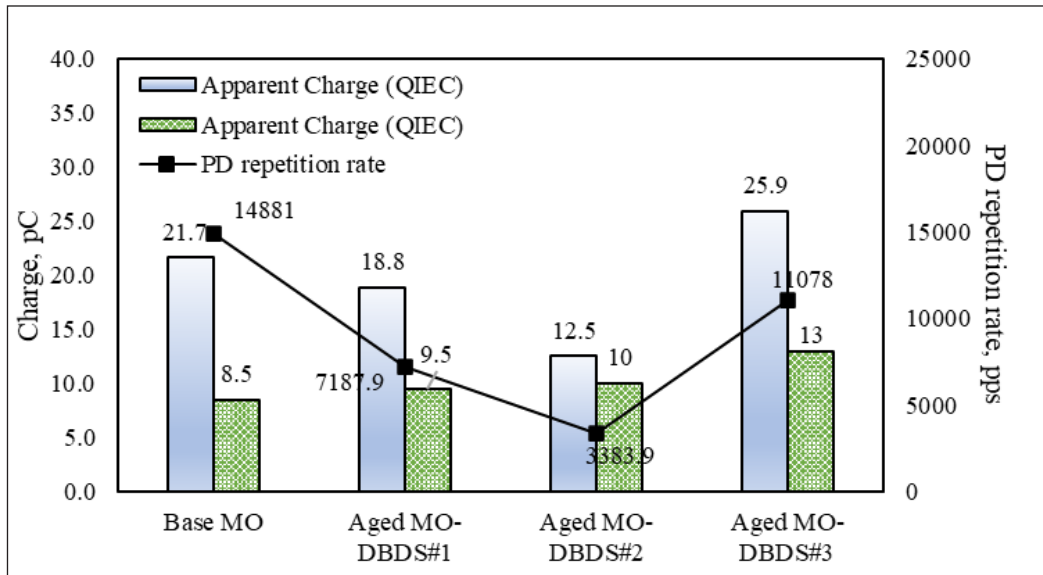


Figure 11. Comparison of the partial discharge characteristics for the base and aged MOs in the presence of DBDS based on plane-plane electrode configuration at 10 mm gap distance

The apparent charge of aged MO shows no clear pattern as the DBDS concentration increases for plane-plane electrode configuration for a 20 mm gap distance, as shown in Figure 12. As the DBDS increases to 10,000 ppm, the apparent charge of aged MO fluctuates between 10.8% and 34.7% compared to base MO. There is no clear pattern for the average charge of aged MO as the DBDS concentration increases. The apparent charge of aged MO maintains close to 20 pC as the DBDS concentration increases by 10,000 ppm. The PD repetition rate of aged MO shows a slight increment pattern whereby the highest increment percentage can be up to 14.8% at a DBDS concentration of 10,000 ppm.

Table 4 summarises the skewness and kurtosis of PD apparent charge, average charge, and PD repetition rate for plane-plane electrode configuration. At a 10 mm gap, the skewness of apparent charge stays for all MO samples consistently low, which indicates uniform data, while kurtosis varies, with peaks for aged MO at DBDS concentrations

of 1,000 ppm and 5,000 ppm and flat distributions in base MO and aged MO at DBDS concentration of 10,000 ppm. The average charge skewness shifts slightly from right- to left-skewed as the DBDS concentration increases, with kurtosis increases for aged MO at a DBDS concentration of 10,000 ppm, which indicates extreme data. The PD repetition rate skewness of all MO samples stays low and slightly positive, with kurtosis increasing for aged MO at a DBDS concentration of 5,000 ppm and decreasing for MO at a DBDS concentration of 10,000 ppm.

At a 20 mm gap, the apparent charge skewness shifts from right-skewed in base MO to nearly symmetrical and left-skewed as the DBDS concentration increases for aged MO. The kurtosis peaks for aged MO at a DBDS concentration of 5,000 ppm DBDS and decreases for aged MO at a DBDS concentration of 10,000 ppm. The average charge starts right skewed in base MO and becomes symmetrical as the DBDS concentration increases for aged MO, with the kurtosis being the highest for base MO and decreasing for aged MOs with DBDS. The PD repetition rate skewness stays slightly negative, while kurtosis is high for base MO and decreases as the DBDS increases, which indicates more uniform distributions. These trends reflect the changes in distribution characteristics.

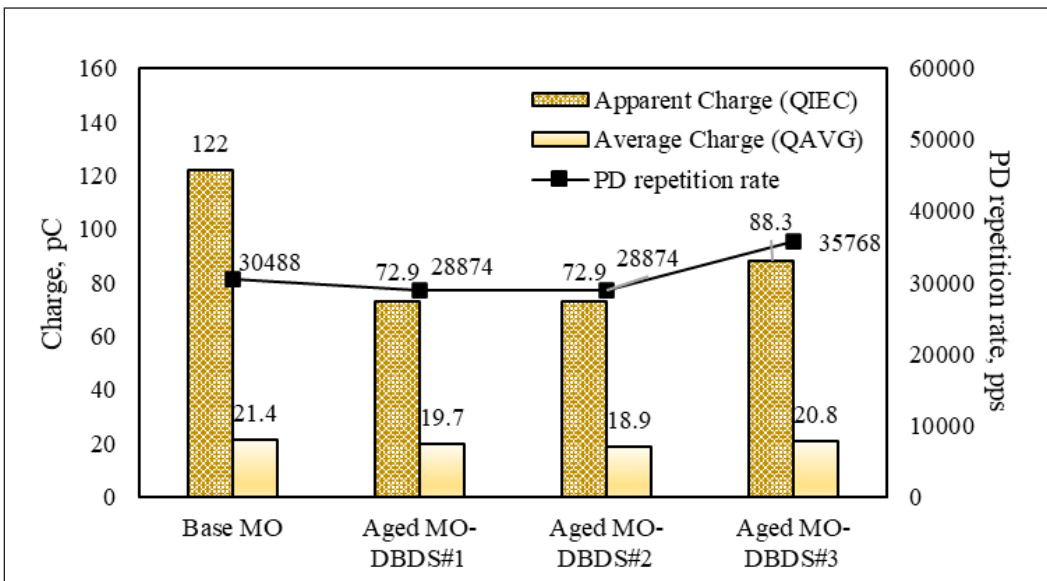


Figure 12. Comparison of the partial discharge characteristics for the base and aged MOs in the presence of DBDS based on plane-plane electrode configuration at 20 mm gap distance

Table 4
Skewness and kurtosis analyses for apparent charge, average charge and partial discharge repetition rate under plane-plane electrode configuration

Parameter	Apparent charge			Average Charge			PD repetition rate				
	Base MO	Aged MO- DBDS#1	Aged MO- DBDS#2	Base MO	Aged MO- DBDS#1	Aged MO- DBDS#2	Base MO	Aged MO- DBDS#1	Aged MO- DBDS#2	Aged MO- DBDS#3	
Skewness - 10 mm	-0.3	-7.8	-6.8	-1.0	-1.0	-1.1	-2.9	2.5	3.8	3.9	1.0
Kurtosis - 10 mm	-0.6	74.0	46.7	1.1	-1.3	1.3	6.6	12.0	16.6	20.6	6.0
Skewness - 20 mm	1.5	0.2	-0.7	-0.1	-1.5	-1.6	-1.6	-7.3	-3.6	-4.9	-3.7
Kurtosis - 20 mm	0.9	-0.5	0.9	-0.3	1.1	1.3	1.2	83.4	14.9	30.3	15.6

The PDIV increment patterns for aged MOs with the increment of DBDS concentration are quite clear for needle-sphere and needle-plane electrode configurations compared to plane-plane electrode configurations at a 10 mm gap distance, as shown in Figure 13. The highest increment of PDIV is found at a DBDS concentration of 10,000 ppm for both electrode configurations. The highest percentages of PDIV increments for aged MO under needle-sphere, needle-plane and plane-plane electrode configurations are 89.0%, 85.7% and 31.5%.

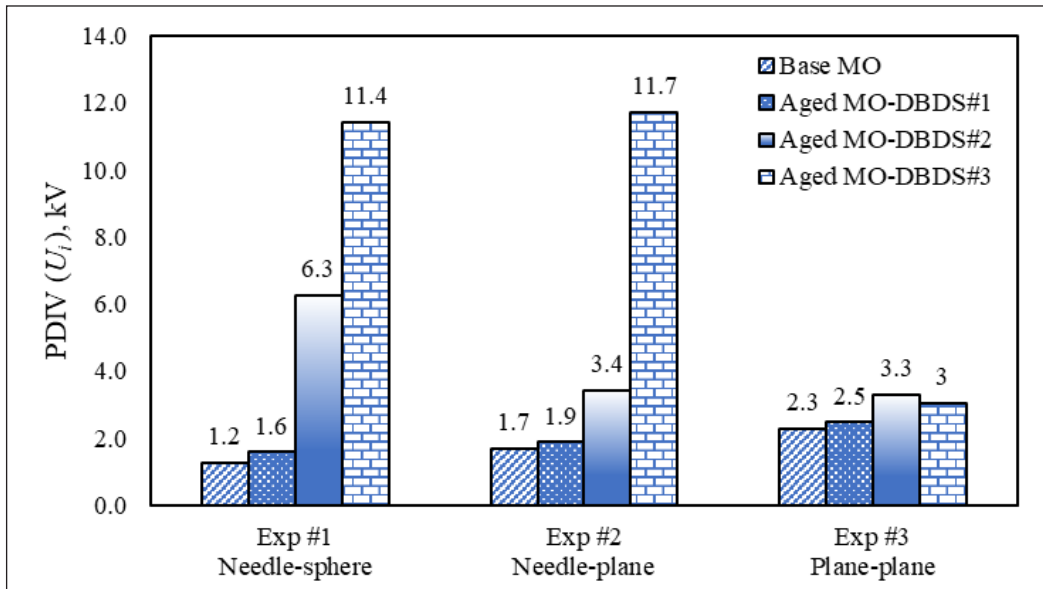


Figure 13. Partial discharge inception voltage, U_i at 10 mm gap distance

The PDIV patterns for aged MO at a 20 mm gap distance are quite similar for all electrode configurations in the presence of DBDS, as shown in Figure 14. For needle-sphere and needle-plane electrode configurations, the PDIVs of aged MOs show a decrement pattern as the DBDS concentration increases to 5,000 ppm. The PDIVs of aged MOs slightly increase at the DBDS concentration of 10,000 ppm. The PDIV of aged MO shows an increment pattern for plane-plane electrode configuration as the DBDS concentration increases. The PDIVs of aged MO for needle-sphere and needle-plane electrode configurations experience the highest reduction of 55.1% and 47.3% at DBDS concentrations of 1,000 ppm and 5,000 ppm. The highest increment of PDIV for aged MO is 31.7% at a DBDS concentration of 5,000 ppm for plane-plane electrode configuration. In conclusion, at both gap distances, the increment pattern of PDIV due to the increment of DBDS concentrations somehow exhibits a similar increment pattern in the presence of moisture as compared to when it is in the dry condition as studied in Jaroszewski and Rakowiecki (2017) and Liu et al. (2014).

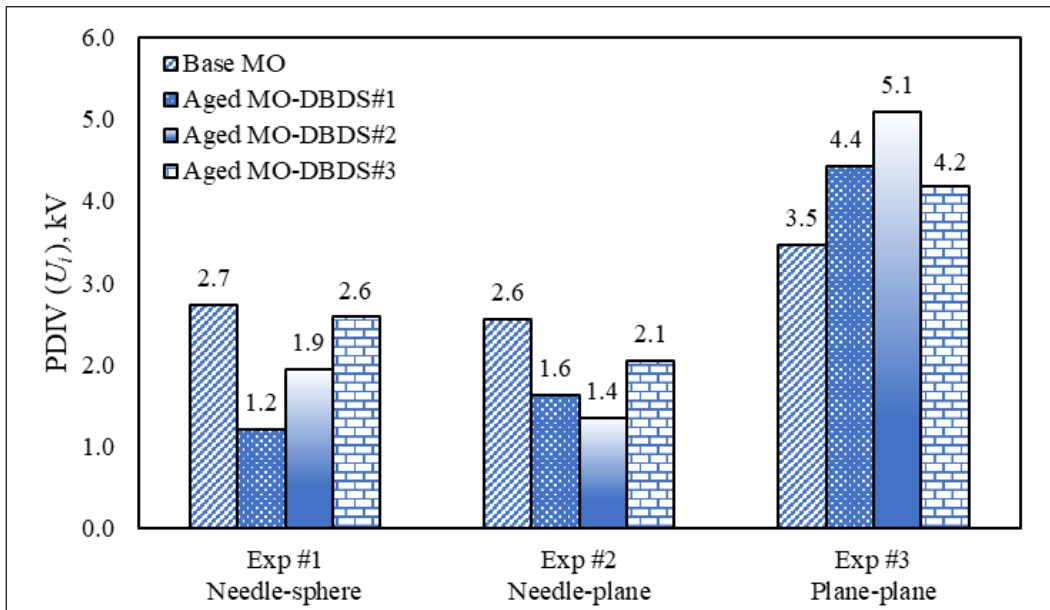


Figure 14. Partial discharge inception voltage, U_i at 20 mm gap distance

At a 10 mm gap distance, it is found that the PDs of aged MO start to initiate in correspondence to negative peak half-wave between 225° and 290° from the 3rd to 4th quadrants and are undetectable at positive half-wave for all electrode configurations as shown in Figures 15 to 17. The patterns of PD intensity, $H_n(\varphi)$ of aged MO, are distributed along apparent charge, Q_{IEC} of 10 pC at all electrode configurations for both base and aged MOs with the increment of DBDS concentrations whereby no obvious shape is observed. However, it is observed that there is an enlargement of the PRPD pattern's shape for aged MO at DBDS concentration of 10,000 ppm under needle-plane and plane-plane electrode configurations, as shown in Figures 16(d) and 17(d), respectively.

At 20 mm gap distance, the PD of aged MO tends to increase predominantly in correspondence to negative peak half-wave between 200° and 315° from 3rd to 4th quadrants and undetectable at positive half-wave for all electrode configurations as shown in Figures 18 to 20. The patterns of PD intensity, $H_n(\varphi)$ for needle-plane electrode configuration, are distributed along the apparent charge, Q_{IEC} , of 10 pC. However, the PD intensity, $H_n(\varphi)$ for needle-sphere and plane-plane electrode configurations are distributed between apparent charge, Q_{IEC} from 5 pC to 100 pC. The asymmetric shape of PRPD patterns for base and aged MOs at different DBDS concentrations in all electrode configurations for both gap distances suggest a Type 5 PRPD pattern due to strong discharge in the negative half-wave and negligible discharges in the positive half-wave. This pattern is often associated with non-conductive cavities in insulation materials like oil or solid dielectrics (eCIGRE, 2017).

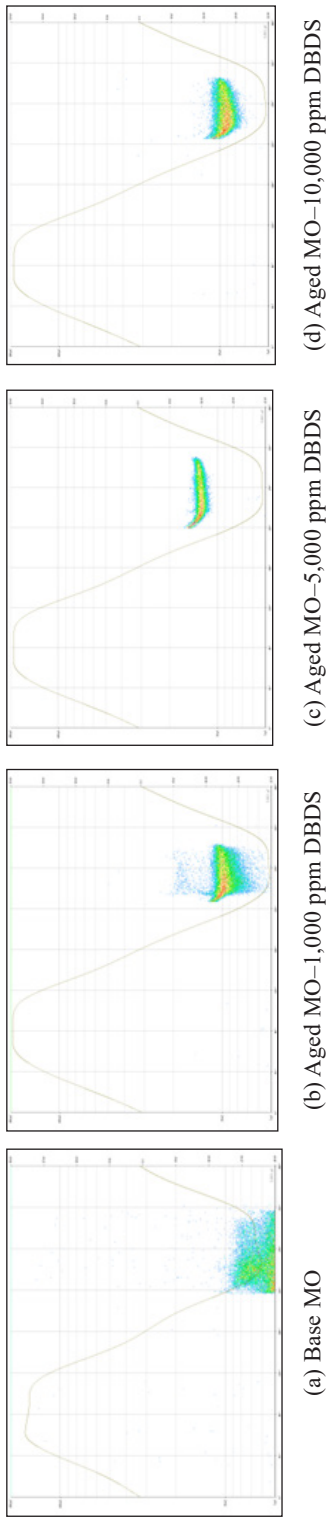


Figure 15. PRPD pattern for needle-sphere electrode configuration at 10 mm gap distance for 250kHz \pm 150kHz (IEC 60270)

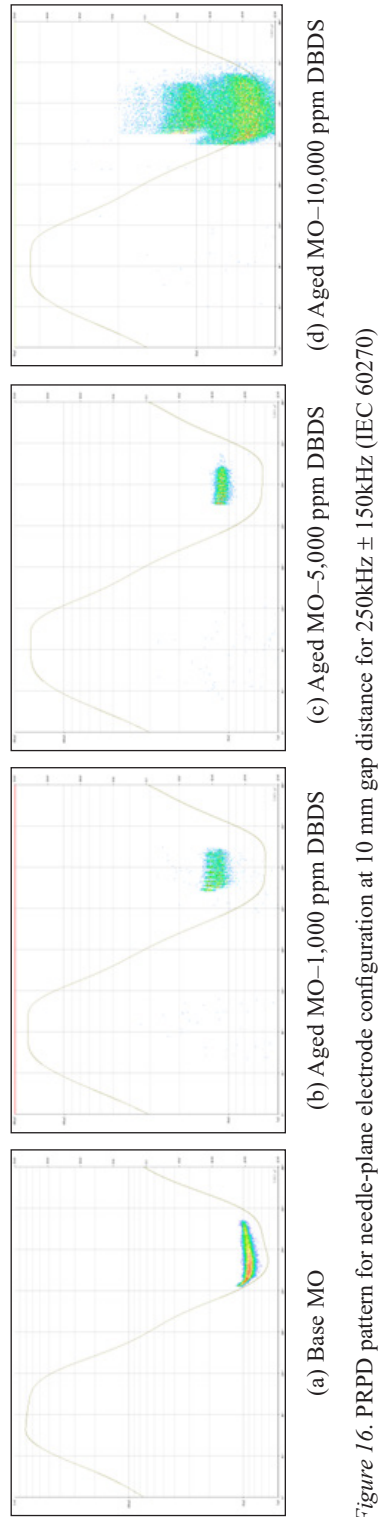


Figure 16. PRPD pattern for needle-plane electrode configuration at 10 mm gap distance for 250kHz \pm 150kHz (IEC 60270)

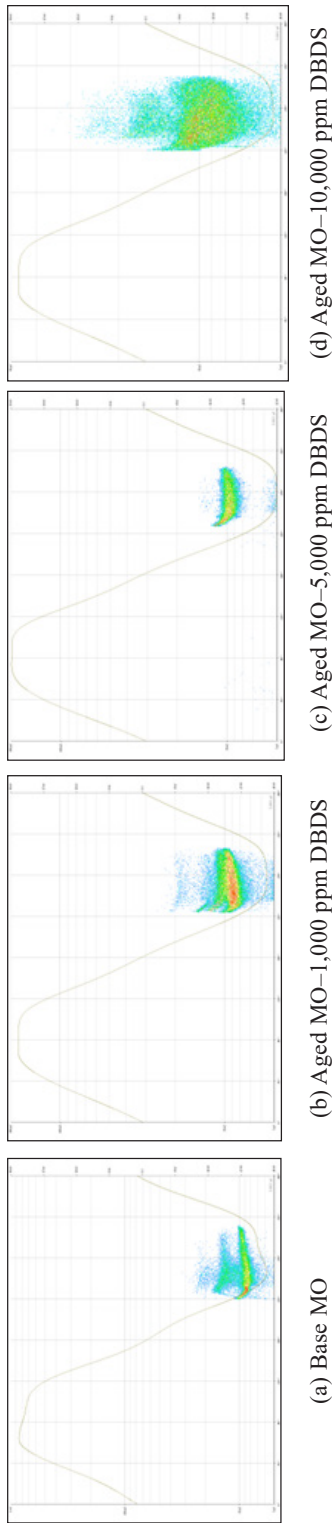


Figure 17. PRPD pattern for plane-plane electrode configuration at 10 mm gap distance for 250kHz \pm 150kHz (IEC 60270)

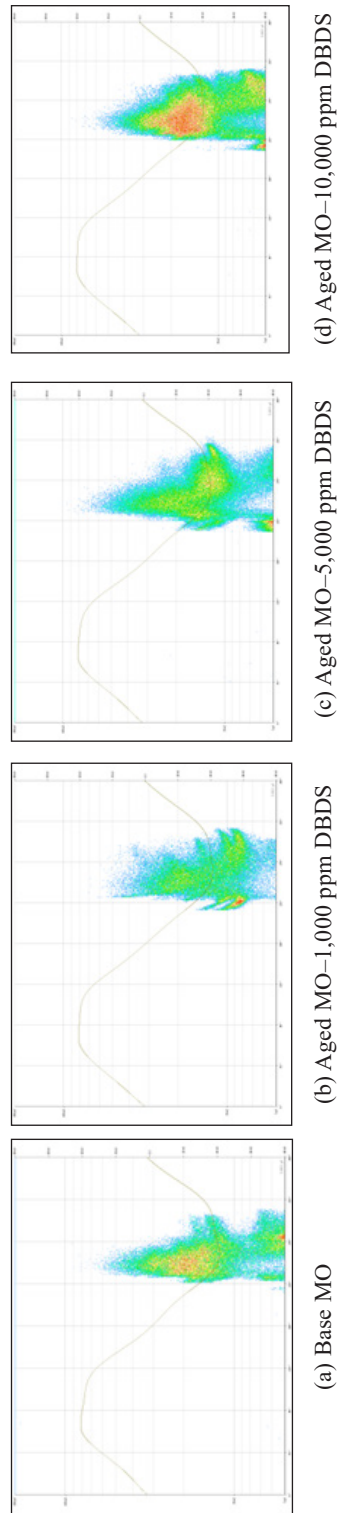


Figure 18. PRPD pattern for needle-sphere electrode configuration at 20 mm gap distance for 250kHz \pm 150kHz (IEC 60270)

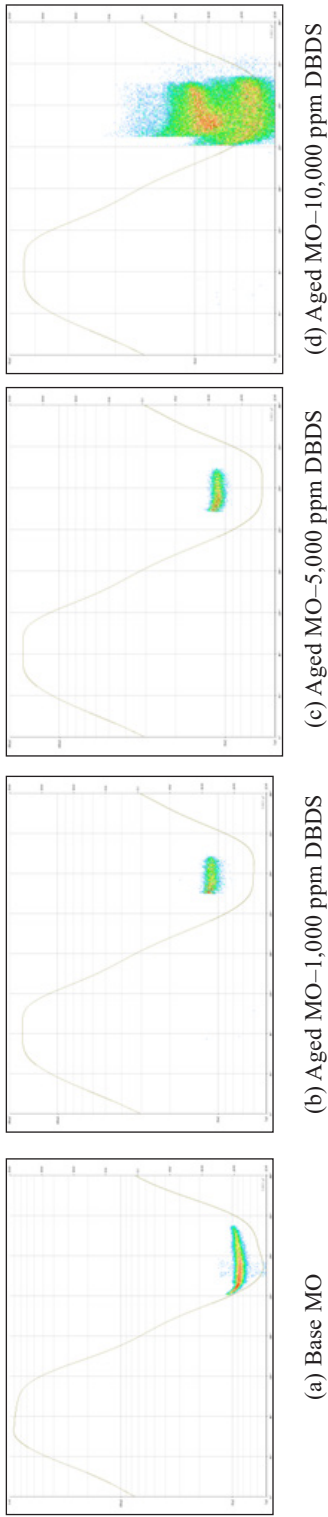


Figure 19. PRPD pattern for needle-plane electrode configuration at 20 mm gap distance for 250kHz \pm 150kHz (IEC 60270)

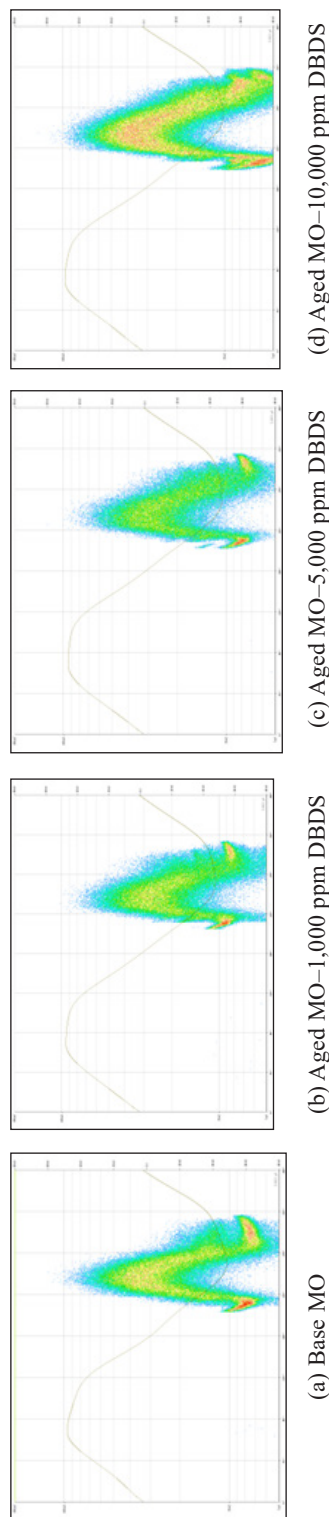


Figure 20. PRPD pattern for plane-plane electrode configuration at 20 mm gap distance for 250kHz \pm 150kHz (IEC 60270)

It is important to observe that the discharge is found to predominantly occur in the negative half-wave for the base and aged MOs as well as dielectric insulating fluids that contain nanoparticles, as investigated by other works (Atiya et al., 2020; Sangineni et al., 2023). During the positive half-wave, the electric field might not be strong enough to cause significant ionisation and discharges. Negative charges accumulate in the defects at the negative half-wave, which provides better conditions for PDs. Positive charges have lower mobility than negative charges. The shape of the electrodes also affects how the electric field is distributed. Electric fields distribute ununiformly for positive half-wave, which leads to low stress near defects, especially for needle-plane electrode configuration. Also, MO with DBDS can behave non-linearly in high electric fields, leading to high discharge in the negative half-wave (Pompili & Bartnikas, 2014; Roslan et al., 2023).

CONCLUSION

The AC breakdown voltages of aged MOs generally show a decrement pattern as the concentration of DBDS increases for all electrode configurations and gap distances. The apparent and average charges of aged MOs show increment patterns as the DBDS concentration increases. The PD repetition rate of aged MO shows fluctuation patterns for all electrode configurations in the presence of DBDS. The data across various electrode configurations and gap distances show that the increment of DBDS concentration in MO can affect the skewness and kurtosis of PD apparent charge, average charge, and PD repetition rate, indicating symmetry and distribution uniformity shifts. The PDIVs of aged MOs show an increment pattern as the DBDS concentration increases for all electrode configurations at a 10 mm gap distance. At a 20 mm gap distance, the increment pattern of PDIVs for aged MOs is found only for plane-plane electrode configuration. It also reveals that the PRPD is asymmetrical for positive and negative half-waves, and discharge mainly concentrates around the negative peak of the applied voltage. The PRPD is undetectable at positive half-wave for both gap distances. The PRPD pattern exhibits a type 5 PD pattern, which indicates non-conducting material, i.e., a cavity without direct contact with the electrode.

ACKNOWLEDGEMENT

This research was funded by Universiti Putra Malaysia, Putra Grant Scheme, Inisiatif Putra Berkumpulan (GP- IPB/2022/9717000).

REFERENCES

- Amalanathan, A. J., Sarathi, R., Zdanowski, M., Vinu, R., & Nadolny, Z. (2023). Review on gassing tendency of different insulating fluids towards transformer applications. *Energies*, 16(1), Article 488. <https://doi.org/10.3390/en16010488>
- Amaro, P. S. (2015). *Corrosive Sulphur in Large Transformers: Impact, Quantification and Detection*. (Doctoral dissertation). Universiti of Southampton, UK. <https://eprints.soton.ac.uk/374902/>

- Atiya, E. G., Mansour, D. E. A., & Izzularab, M. A. (2020). Partial discharge development in oil-based nanofluids: Inception, propagation and time transition. *IEEE Access*, 8, 181028–181035. <https://doi.org/10.1109/ACCESS.2020.3027905>
- Bramantyo, A. P., Ciani, F., Serra, S., Morshuis, P. H. F., Cavallini, A., & Montanari, G. C. (2014). Experimental investigation on the role of corrosive sulphur on the development of partial discharges in power transformers. In *Proceedings of 2014 International Symposium on Electrical Insulating Materials* (pp. 136-139). IEEE Publishing. <https://doi.org/10.1109/ISEIM.2014.6870739>
- Cong, H., Pan, H., Qian, D., Zhao, H., & Li, Q. (2021). Reviews on sulphur corrosion phenomenon of the oil–paper insulating system in mineral oil transformer. *High Voltage*, 6(2), 193-209. <https://doi.org/10.1049/hve.2020.0060>
- Cong, H., Qiao, L., Wang, Y., Hu, X., Su, W., Lian, H., & Li, Q. (2024). Effect of copper sulfide deposition on the partial discharge of oil-paper insulation under plate-plate electrodes. *IEEE Transactions on Dielectrics and Electrical Insulation*, 31(2), 824–833. <https://doi.org/10.1109/TDEI.2023.3332052>
- Cong, H., Zhang, M., & Li, Q. (2018). Study on sulfide distribution in the operating oil of power transformers and its effect on the oil quality. *Applied Sciences*, 8(9), Article 1577. <https://doi.org/10.3390/app8091577>
- Dixit, A., & Samarasinghe, S. (2019). Comparative study of partial discharge (PD) signal characteristics in insulation systems filled with mineral and ester oil. In *2019 IEEE Innovative Smart Grid Technologies-Asia (ISGT Asia)* (pp. 3849-3854). IEEE Publishing. <https://doi.org/10.1109/ISGT-Asia.2019.8880928>
- eCIGRE. (2009). Copper Sulphide in Transformer Insulation. CIGRE. <https://www.e-cigre.org/publications/detail/378-copper-sulphide-in-transformer-insulation.html>
- eCIGRE. (2017). Partial Discharges in Transformers. CIGRE. <https://www.e-cigre.org/publications/detail/676-partial-discharges-in-transformers.html>
- Flora, S. D., & Rajan, J. S. (2016). Assessment of paper-oil insulation under copper corrosion using polarization and depolarization current measurements. *IEEE Transactions on Dielectrics and Electrical Insulation*, 23(3), 1523–1533. <https://doi.org/10.1109/TDEI.2016.005577>
- Gao, S. H., Yang, L. J., & Ding, D. (2019). Corrosion mechanism for copper sulfide formation induced by dibenzyl disulfide in oil-immersed insulation. *IEEE Access*, 7, 23100–23108. <https://doi.org/10.1109/ACCESS.2019.2894125>
- Hu, E., Yang, L., Liao, R. J., Liu, Y., & Yuan, Y. (2016). Effect of an electric field on copper sulphide deposition in oil-impregnated power transformers. *IET Electric Power Applications*, 10(3), 155–160. <https://doi.org/10.1049/iet-epa.2015.0018>
- Jadim, R., Kans, M., Rehman, S., & Alhems, L. M. (2020). A relevant condition monitoring of corrosive sulphur deposition on the windings of oil-filled electrical transformers. *IEEE Transactions on Dielectrics and Electrical Insulation*, 27(5), 1736–1742. <https://doi.org/10.1109/TDEI.2020.008955>
- Janani, H., Shahabi, S., & Kordi, B. (2020). Separation and classification of concurrent partial discharge signals using statistical-based feature analysis. *IEEE Transactions on Dielectrics and Electrical Insulation*, 27(6), 1933–1941. <https://doi.org/10.1109/TDEI.2020.009043>

- Jaroszewski, M., & Rakowiecki, K. (2017). Partial discharge inception voltage in transformer natural ester liquid - Effect of the measurement method in the presence of moisture. *IEEE Transactions on Dielectrics and Electrical Insulation*, 24(4), 2477–2482. <https://doi.org/10.1109/TDEI.2017.005917>
- Jin, H., Morshuis, P., Mor, A. R., Smit, J. J., & Andritsch, T. (2015). Partial discharge behavior of mineral oil based nanofluids. *IEEE Transactions on Dielectrics and Electrical Insulation*, 22(5), 2747–2753. <https://doi.org/10.1109/TDEI.2015.005145>
- Khan, F., & Rajan, J. (2015). Experimental simulation of effects of copper sulphide on insulation system of transformers. *IEEE Transactions on Dielectrics and Electrical Insulation*, 22(1), 571–580. <https://doi.org/10.1109/TDEI.2014.004408>
- Khlar, M. S. A., Brown, R. C. D., & Lewin, P. L. (2019). Sacrificial copper strip sensors for sulfur corrosion detection in transformer oils. *Measurement: Journal of the International Measurement Confederation*, 148, Article 106887. <https://doi.org/10.1016/j.measurement.2019.106887>
- Khlar, M. S. A., Garcia, S., Lewin, P. L., Brown, R. C. D., Pilgrim, J. A., Langley, G. J., & Wilson, G. (2020). On-line quantification of corrosive sulphur content in large autotransformers. *IEEE Transactions on Dielectrics and Electrical Insulation*, 27(6), 1787–1794. <https://doi.org/10.1109/TDEI.2020.008548>
- Liao, R., Hu, E., Yang, L., & Yuan, Y. (2015). Space charge behavior in paper insulation induced by copper sulfide in high-voltage direct current power transformers. *Energies*, 8(8), 8110–8120. <https://doi.org/10.3390/en8088110>
- Liu, Z., Liu, Q., Wang, Z. D., Jarman, P., Krause, C., Smith, P. W. R., & Gyore, A. (2014). Partial discharge behaviour of transformer liquids and the influence of moisture content. In *2014 IEEE 18th international conference on dielectric liquids (ICDL)* (pp. 1-4). IEEE Publishing. <https://doi.org/10.1109/ICDL.2014.6893155>
- Ma, S., Yang, D., Liang, B., & Jin, Y. (2019). Impact of metal particle size on partial discharge characteristics of moving metal particles in transformer oil. *Chemical Physics Letters*, 731, Article 136577. <https://doi.org/10.1016/j.cplett.2019.07.005>
- Pattanadech, N., & Muhr, M. (2016). Partial discharge inception voltage investigation of mineral oil: Effect of electrode configurations and oil conditions. *IEEE Transactions on Dielectrics and Electrical Insulation*, 23(5), 2917–2924. <https://doi.org/10.1109/TDEI.2016.7736853>
- Pompili, M., & Bartnikas, R. (2014). Gas formation in transient cavities undergoing PD pulse burst discharges in transformer oils. *IEEE Transactions on Plasma Science*, 42(6), 1697–1703. <https://doi.org/10.1109/TPS.2014.2317847>
- Rehman, S., Alhems, L. M., Jadim, R., Al Faraj, B. A., Balasubramanian, K. S., Al Mutairi, K. S., Al-Yemni, A. K., Shinde, D. V., & Al-Hsaien, S. A. (2016). Maximum acceptable concentrations of dbds, sulphur mercaptan and optimal concentration of passivators for safe and prolonged operation of power transformers. *IEEE Transactions on Dielectrics and Electrical Insulation*, 23(4), 2438–2442. <https://doi.org/10.1109/TDEI.2016.7556523>
- Rehman, S., Alhems, L. M., Jadim, R., Faraj, B. A. A., Mutairi, K. S. A., & Al-Yemni, A. K. (2017). Experimental investigation of temperature effect on corrosive sulfur formation in transformers. *IEEE Transactions on Dielectrics and Electrical Insulation*, 24(5), 3201–3206. <https://doi.org/10.1109/TDEI.2017.006024>

- Roslan, M. H., Azis, N., Kadir, M. Z. A. A., Jasni, J., & Yousof, M. F. M. (2023). The influence of cavity size and location within insulation paper on the partial discharge activities. *Pertanika Journal of Science and Technology*, 31(6), 2915–2930. <https://doi.org/10.47836/pjst.31.6.15>
- Sangineni, R., Chandrasekaran, T., & Nayak, S. K. (2023). Study of partial discharges in fresh and oxidative aged mineral-natural ester blended oils. *IEEE Transactions on Dielectrics and Electrical Insulation*, 30(5), 2325–2333. <https://doi.org/10.1109/TDEI.2023.3308531>
- Scatiggio, F., Pompili, M., & Bartnikas, R. (2011). Effects of metal deactivator concentration upon the gassing characteristics of transformer oils. *IEEE Transactions on Dielectrics and Electrical Insulation*, 18(3), 701-706. <https://doi.org/10.1109/TDEI.2011.5931055>
- Selva, A. M., Azis, N., Kadir, M. Z. A. A., Jasni, J., Zainuddin, H., & Yousof, M. F. M. (2024). Morphological study on corrosive sulphur development in transformer windings. In *2024 IEEE 4th International Conference in Power Engineering Applications (ICPEA)* (pp. 197-200). IEEE Publishing. <https://doi.org/10.1109/ICPEA60617.2024.10498156>
- Sima, W., Jiang, C., Lewin, P., Yang, Q., & Yuan, T. (2013). Modeling of the partial discharge process in a liquid dielectric: Effect of applied voltage, gap distance, and electrode type. *Energies*, 6(2), 934–952. <https://doi.org/10.3390/en6020934>
- Tang, J., Zhang, Y., Pan, C., Zhuo, R., Wang, D., & Li, X. (2018). Impact of oil velocity on partial discharge characteristics induced by bubbles in transformer oil. *IEEE Transactions on Dielectrics and Electrical Insulation*, 25(5), 1605–1613. <https://doi.org/10.1109/TDEI.2018.006888>
- Toyama, S., Tanimura, J., Yamada, N., Nagao, E., & Amimoto, T. (2009). Highly sensitive detection method of dibenzyl disulfide and the elucidation of the mechanism. *IEEE Transactions on Dielectrics and Electrical Insulation*, 16(2), 509–515. <https://doi.org/10.1109/TDEI.2009.4815186>
- Vahidi, F., & Tenbohlen, S. (2015). *Statistical Failure Analysis of European Substation Transformers*. ResearchGate.
- Wang, X. (2011). *Partial Discharge Behaviours and Breakdown Mechanisms of Ester Transformer Liquids Under AC Stress*. (Doctoral dissertation). University of Manchester, UK. <https://www.escholar.manchester.ac.uk/uk-ac-man-scw:136066>
- Yang, L., Ding, D., Yuan, Y., Gao, S., & Lu, Y. (2022). Influence of contact layer on the sulphur corrosion of copper conductors in power transformers. *High Voltage*, 7(1), 176–184. <https://doi.org/10.1049/hve2.12088>
- Yuan, Y., Gao, X., Zhou, J., Liu, G., Kuang, X., Yang, L., & Liao, R. (2022). A review: Research on corrosive sulphur in electrical power equipment. *High Voltage*, 7(2), 209–221). <https://doi.org/10.1049/hve2.12155>